2-2014

100 kHz thousand-frame burst-mode planar imaging in turbulent flames

James B. Michael
Iowa State University

Prabhakar Venkateswaran
Iowa State University

Joseph D. Miller
Air Force Research Laboratory

Mikhail N. Slipchenko
Spectral Energies

James R. Gord
Air Force Research Laboratory

See next page for additional authors

100 kHz thousand-frame burst-mode planar imaging in turbulent flames

James B. Michael,[1] Prabhakar Venkateswaran,[1] Joseph D. Miller,[3] Mikhail N. Slipchenko,[2] James R. Gord,[3] Sukesh Roy,[2] and Terrence R. Meyer[1,*]

[1]Iowa State University, Department of Mechanical Engineering, Ames, Iowa 50011, USA

[2]Spectral Energies, LLC, Dayton, Ohio 45431, USA

[3]Air Force Research Laboratory, Aerospace Systems Directorate, Wright-Patterson AFB, Ohio 45433, USA

*Corresponding author: trm@iastate.edu

Received October 25, 2013; revised December 17, 2013; accepted December 23, 2013; posted January 3, 2014 (Doc. ID 198353); published February 3, 2014

High-repetition-rate, burst-mode lasers can achieve higher energies per pulse compared with continuously pulsed systems, but the relatively few number of laser pulses in each burst has limited the temporal dynamic range of measurements in unsteady flames. A fivefold increase in the range of timescales that can be resolved by burst-mode laser-based imaging systems is reported in this work by extending a hybrid diode- and flashlamp-pumped Nd:YAG-based amplifier system to nearly 1000 pulses at 100 kHz during a 10 ms burst. This enables an unprecedented burst-mode temporal dynamic range to capture turbulent fluctuations from 0.1 to 50 kHz in flames of practical interest. High pulse intensity enables efficient conversion to the ultraviolet for planar laser-induced fluorescence imaging of nascent formaldehyde and other potential flame radicals.

OCIS codes: (120.1740) Combustion diagnostics; (140.3538) Lasers, pulsed; (300.2530) Fluorescence, laser-induced.
http://dx.doi.org/10.1364/OL.39.000739

High-frame-rate, laser-based planar imaging and spectroscopic measurement techniques in unsteady reacting flows have undergone significant advancements in the past decade [1]. This has enabled time-correlated 2D and 3D measurements of reacting-flow parameters for understanding unsteady phenomena such as local ignition and extinction events in turbulent flames, flame propagation through inhomogeneous mixtures, turbulent vortex-flame interactions, and combustion-system dynamics [1,2].

Recent improvements in high-speed-imaging capability have been enabled by high-frame-rate, intensified complementary metal-oxide semiconductor (CMOS) detectors in conjunction with diode-pumped solid-state (DPSS) and burst-mode laser systems. Commercially available DPSS lasers for diagnostics in reacting flows currently achieve average powers up to ~60 W at 355 nm and ~200 W at 532 nm [3]. At a repetition rate of 100 kHz, for example, this allows continuous operation with pulse energies of 0.6 mJ at 355 nm and 2 mJ at 532 nm. The pulse energy at 532 nm is sufficient for high-speed particle-image velocimetry (PIV) measurements of transient fluid–chemistry interactions; however, such pulse energies would fall below the practical limit for planar laser-induced fluorescence (PLIF) of most gaseous species of interest [2]. The limitations of continuously pulsed DPSS laser systems have been addressed, in part, by advancements in burst-mode laser technology. For example, the ~10–100 times higher pulse energies of burst-mode lasers can be used to access a wider range of combustion parameters of interest at higher frame rates, including OH, CH, NO, CH_2O, soot, fuel-tracer concentrations, mixture fraction, and velocity [4–12]. However, a key challenge for burst-mode laser systems has been the short burst duration (up to 200 frames) and, therefore, limited temporal dynamic range (TDR) [4].

In this work, a fivefold increase in the TDR of burst-mode laser systems is reported, and planar imaging of flame radicals with repetition rates up to 100 kHz is demonstrated over a duration of nearly 10 ms (~1000 frames). The TDR reported in the current work and that of previous burst-mode measurements is summarized in Table 1 for comparison [4–7,10–16]. For many turbulent reacting flows of practical interest, a 10 ms time duration represents multiple cycles of fluctuations in the vector and scalar fields under investigation. This makes it possible to track a wide range of turbulent reacting flow phenomena. The maximum resolvable flow frequency, as shown in Table 1 and based on the Nyquist criterion, is given by one-half the pulse repetition rate. The minimum resolvable flow frequency and the lower resolvable limit of recurring flow features are determined wholly by the burst duration.

Table 1. Operating Parameters and Temporal Dynamic Range of Burst-Mode Laser Systems for High-Speed Imaging

Reference	Burst Time (ms)	Max Flow Freq[a] (kHz)	Min Flow Freq[b] (kHz)	TDR[c]
13	0.140	250	7	35
14	0.875	4	1	3.5
15	0.033	500	30	17
16	0.1	500	10	50
5	1.0	50	1	50
7	0.56	25	1.8	14
11	0.01	500	100	5
4	10	10	0.10	100
6	10	5	0.10	50
10	8.75	10	0.114	88
12	30	2.5	0.033	75
This work, 2013	9.8	50	0.10	490

[a]Maximum flow frequencies determined via Nyquist criterion and pulse repetition rate.

[b]Minimum flow frequencies determined by maximum time separation, or total burst duration, for two flow events.

[c]TDR given by ratio of maximum–minimum flow frequencies.

The fivefold extension of the temporal dynamic range is achieved using a hybrid-pumped burst-mode laser system. The laser is a master-oscillator power-amplifier similar in principle to that discussed by Slipchenko *et al.* [4], with the master oscillator comprising a continuously pulsed fiber-amplified chain of low-energy, 12 ns duration pulses at 100 kHz. The master oscillator is fiber coupled into a double-passed electro-optic modulator (EOM), which provides pulse selection and prevents further amplification of the low-level amplified spontaneous emission present at the output of the master oscillator. This EOM can pulse select down to 5 kHz, but for the experiments discussed here, every pulse was passed to give an initial pulse train at 100 kHz.

The hybrid diode- and flashlamp-pumped architecture employed in this work begins with three single-pass diode-pumped stages (two 2 mm Nd:YAG rods and one 5 mm rod). Two single-pass flashlamp-pumped amplifier stages were added in series (9.5 and 12 mm rods) to give an additional gain of up to a factor of seven. The overall system, shown in the schematic diagram of Fig. 1, occupies a small table footprint (0.6 m by 0.9 m). At 100 kHz, the energy at the exit of the three diode-pumped stages is 12 mJ/pulse and the subsequent two-stage flashlamp amplification generates >50 mJ/pulse at 1064 nm for a total burst energy of >60 J/burst. A typical burst profile is shown in the photodiode trace of Fig. 2(a) with a histogram showing RMS pulse-to-pulse fluctuations for the fundamental of ±9% in Fig. 2(b), which are due to the current master oscillator pulse-to-pulse stability. The hybrid diode- and flashlamp-pumped configuration used in this work allows for a relatively flat gain profile for the 10 ms burst duration, which is achieved by careful attention to several operating parameters. The use of three single-pass diode stages along with an optimal rod temperature allows for excellent flatness in the gain profile across the burst while limiting the effect of nonuniform spatial gain in the rods. The final flashlamp-pumped stages are low gain, and the nonuniform temporal gain is limited to <5%. For comparison, an all-flashlamp-pumped system developed by the authors can exhibit a droop of 20% across a 10 ms burst. In addition to burst flatness, the laser exhibits a pointing stability of <50 μrad over the burst.

The peak intensity ($>10\times10^6$ W/cm^2) is sufficient for >50% second-harmonic conversion with a noncritically

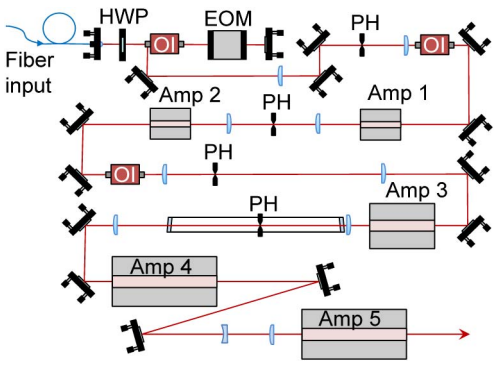

Fig. 1. Burst-mode laser layout. HWP, half-wave plate; EOM, electro-optic modulator; PH, pinhole; Amp, amplifier; TFP, thin-film polarizer; OI, optical isolator.

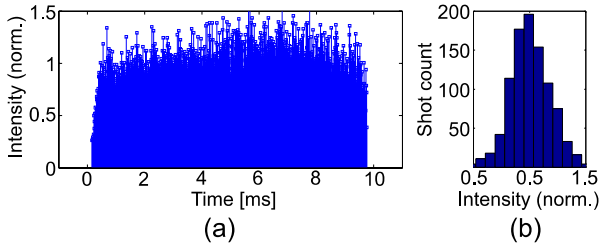

Fig. 2. (a) Fundamental output showing a 980 pulse sequence with ±9% shot-to-shot fluctuations. (b) Histogram of normalized pulse intensities.

phase-matched type-I lithium triborate (LBO) crystal and ~4 mm input beam diameter. Third-harmonic generation of up to 30% is achieved with a type-I LBO crystal after the beam passes through a half-waveplate for 532 nm and a full waveplate for 1064 nm. At these fluences, there is no evidence of harmonic-conversion degradation during the burst, with the conversion efficiency being similar to prior work [4,5,8]. The resulting ultraviolet pulse train of 15 mJ/pulse at 355 nm is unprecedented for burst durations of nearly 1000 pulses, allowing for extended time records of formaldehyde (CH_2O) PLIF at 100 kHz with high signal-to-noise ratio (SNR). This is 25 times the output energy of current state-of-the-art continuously pulsed DPSS laser systems for combustion diagnostics at the same repetition rate.

To evaluate the utility of the laser system, CH_2O PLIF imaging was recorded in a lifted jet diffusion flame, as depicted in Fig. 3, consisting of a 10 mm outer-diameter fuel tube tapered over a distance of 10 mm to an inner diameter of 8 mm. The turbulent jet tube is surrounded by a 125 mm × 125 mm square laminar co-flow section. The jet-exit Reynolds number was 11,000 for a fuel mixture of methane/nitrogen/hydrogen with an 80/15/5 ratio. The lifted jet flame was stabilized at $x/D\sim20$, where the level of turbulence is higher than in an attached jet flame with the same jet-exit Reynolds number. Works by Schefer and Goix [17] and Muñiz and Mungal [18] suggest that the local Reynolds number at the flame base, defined by the jet width and the velocity along

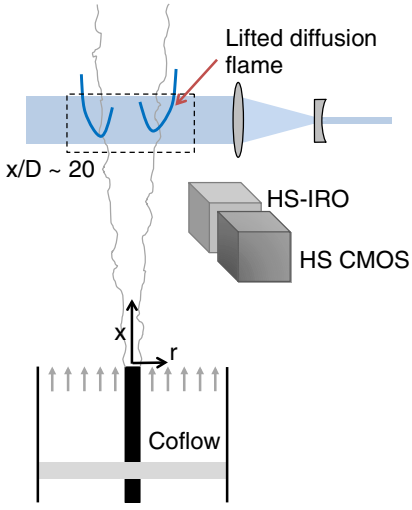

Fig. 3. Experimental setup showing lifted diffusion flame and field of view imaged by HS-IRO and high-speed CMOS imaging system.

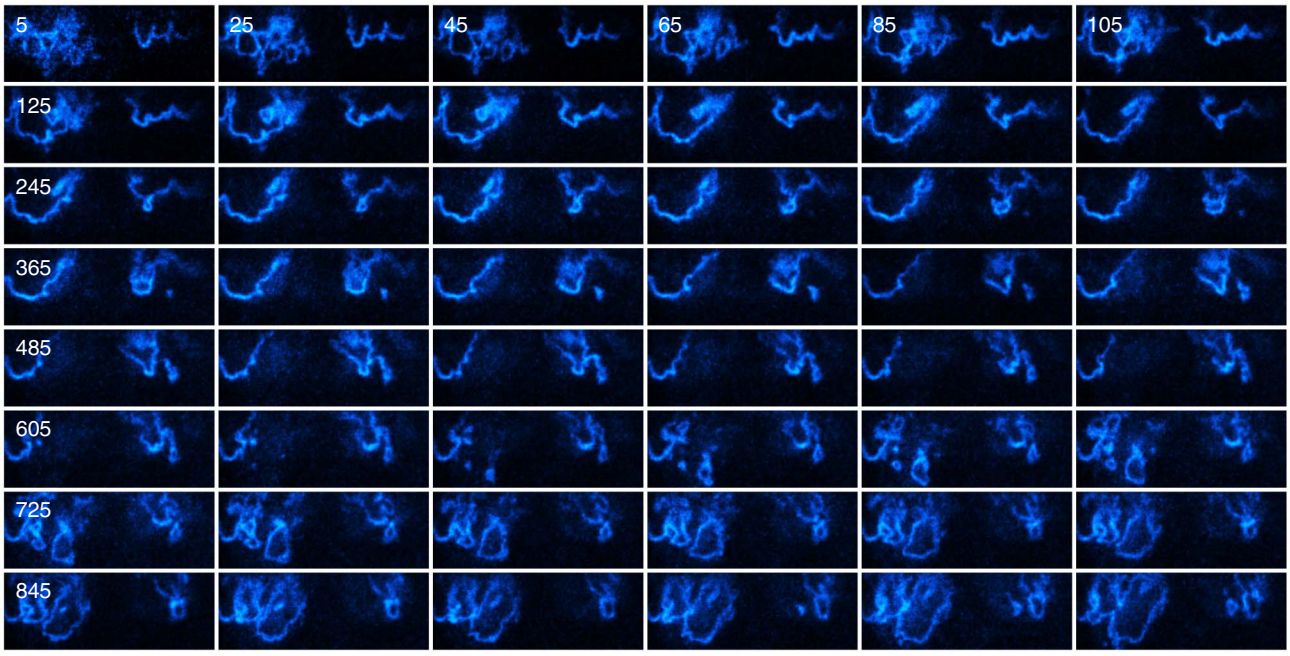

Fig. 4. Sample sequence of CH_2O PLIF at 100 kHz showing every 20th image in record length of 980 images (video of complete sequence shown in Media 1). Typical signal levels indicated in line plots of Fig. 5 below.

the centerline, is approximately equal to the jet-exit Reynolds number. This level of turbulence is evident in the time-evolution of formaldehyde structures in the 100 kHz image sequence presented in Fig. 4.

The formaldehyde PLIF excitation was achieved with the third harmonic of the burst-mode Nd:YAG near 355 nm through excitation of a weak overtone of the A–X band of CH_2O, which has a bandhead at 353 nm [19]. The formaldehyde PLIF images were acquired with a LaVision High-Speed Imaging Relay Optic (HS-IRO) intensifier coupled to a Photron SA-5 high-speed CMOS camera. Images were acquired with a 58 mm, $f/1.2$ Nikon lens with a 12 mm lens tube extension. A bandpass filter from 370 to 450 nm and a 100 ns HS-IRO time gate were used to limit both laser scattering and flame chemiluminescence, respectively. With this objective and the 100 kHz repetition rate, the image was limited to a region of 320 by 192 pixels, with a cropped field of view of 25 mm by 71 mm. This magnification gives 220 μm/pixel, which is smaller than the laser sheet thickness (~550 μm) measured by a scanning knife-edge technique. A collimated laser sheet of 25 mm in height was formed at $x/D \sim 20$ using a −100 mm focal-length cylindrical concave lens and a +500 mm focal-length spherical lens.

Using the hybrid diode- and flashlamp-pumped architecture laid out above, a sequence of 980 formaldehyde PLIF images was obtained, from which every 20th frame of the sequence is presented (Fig. 4). The typical SNR achieved in each image is ~30, which is defined by signal levels in the formaldehyde layers and background noise. Three horizontal locations in the CH_2O layer at the flame base are indicated with dashed lines in Fig. 5(a) with the accompanying profiles shown in Fig. 5(b) to illustrate SNR in the images, which are background subtracted and normalized by shot-to-shot laser energies.

A potential concern for imaging with high-speed intensifiers is the finite phosphor decay time. The IRO phosphor lifetime was measured by illuminating the input with diffuse laser scatter at 100 kHz and monitoring the phosphor-screen signal level with a photomultiplier tube (Hamamatsu 931B). The phosphor signal was found to drop 99% within 5 μs, which compares favorably with the manufacturer's 3 μs specification. In addition, intensifier depletion is a concern at high-repetition rates where charge cannot be replenished quickly enough. This effect is a function of total output of the IRO. For the output signal levels in this experiment, the error due to depletion effects, also measured at 100 kHz with a PMT, was less than 5%. It appears from the formaldehyde layer thicknesses, both normal to and in the direction of flame propagation, that these effects are negligible for the current conditions.

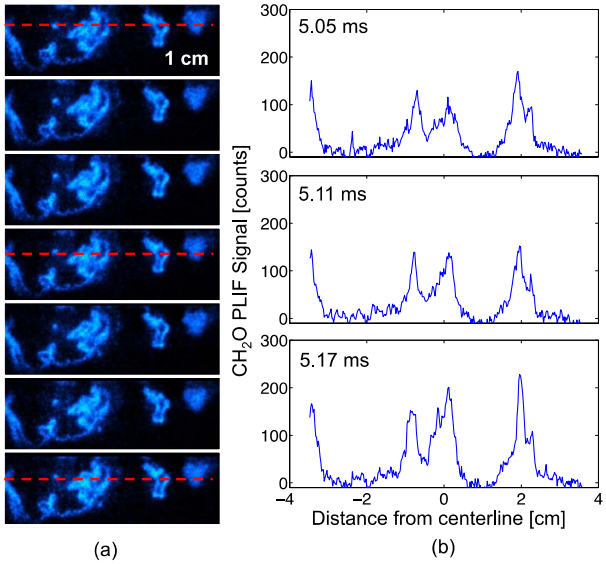

Fig. 5. (a) Sample formaldehyde PLIF images every 20 μs and (b) line plots across three images of interest.

As shown in Table 1, the image series reported in this work represents a fivefold improvement in TDR over prior burst-mode PLIF measurements, which have been limited either in burst duration or repetition rate [4–16]. The measured SNR of 30 without pixel binning is comparable to those previously reported pulse-burst formaldehyde PLIF sequences [4,12] as well as to those in which pixel binning was employed [8].

To evaluate the utility of this new measurement capability, it is of interest to consider the range of relevant timescales in the current as well as other potential applications. By examining the 100 kHz time series, it is evident that the motion of large-scale formaldehyde structures within the field of view can occur over a few ms, including movement of the flame-stabilization point. This type of bulk motion is visible in each column of Fig. 4, where the flame position shifts across the 25 mm vertical extent of the field of view. The centerline velocity and the spatial extent of the field of view in the vertical direction can be used to estimate the timescale of this bulk motion. Following classical scaling for nonreacting turbulent axisymmetric jets, the centerline velocity scales as $U_c(x)/U_0 = 6(D/x)$ [20]. At the stabilization point for this flame, the centerline velocity for a nonreacting jet is approximately 12 m/s, and large-scale structures should propagate through the vertical field of view within a time duration of approximately 2 ms or longer. Hence, the 10 ms burst duration is sufficient to track such large-scale motions, as well as a wide range of lower convection velocities that may be present within the flow.

Of course, the motion of individual flame layers has a much faster timescale. Significant movement between frames is observed with time delays of 50 to 100 μs, where the autocorrelation between images drops below one half. This evolution can also be seen in the fine structures of Fig. 5(a), where each image is separated in time by 20 μs. The shift in structures across a horizontal line in the frames, as shown in Fig. 5(b), reveals changes in layer widths and signal amplitudes even for the relatively moderate turbulence level reported here. Applications in practical propulsion systems require measurements in facilities where flow velocities can be of the order 100 m/s. At such speeds and with the current temporal resolution of 10 μs, flame structures with this velocity would propagate a distance of ~1 mm/frame and could be tracked in detail during the time sequence before exiting the 25 mm field of view. Many of these systems also exhibit low-frequency combustion instabilities, from longitudinal to transverse acoustic modes that typically fall in the range 100 Hz to 5 kHz [21]. From these timescales of interest, it is evident that a 100 kHz, 10 ms burst-mode image sequence can cover a wide TDR of practical interest, including convective temporal scales and instabilities for dynamical system analysis over a broad range of conditions.

As with prior burst-mode measurements, the spatial resolution is limited to several times the typical diffusion length scale for turbulent conditions. Improvements can be achieved by employing image magnification and through advances in camera technology. Currently, only a small portion of the image intensifier is utilized because the camera limits the size of the region on the CMOS sensor that can be utilized at high repetition rates.

In conclusion, PLIF imaging of formaldehyde, a key combustion intermediate, has been demonstrated in turbulent flames at a frame rate of 100 kHz for a burst duration of nearly 10 ms. The record length of nearly 1000 images enables a fivefold increase in the temporal dynamic range of burst-mode planar measurements, allowing investigation of flow features with frequencies in the range of 100 Hz to 50 kHz. The combination of high repetition rate and longer burst duration opens new opportunities to investigate unsteady phenomena in practical combustion systems, such as flame stabilization, extinction, propagation, and nonlinear dynamics.

Funding for this work was provided by the Air Force Office of Scientific Research (Chiping Li, Program Manager) and the Air Force Research Laboratory under contract no. FA8650-12-C-2200. The authors are also grateful for technical assistance from Daniel Diaz, Mark Johnson, and Allen Barrow of Iowa State University.

References

1. B. Böhm, C. Heeger, R. L. Gordon, and A. Dreizler, Flow Turbul. Combust. **86**, 313 (2010).
2. I. Boxx, C. D. Carter, M. Stöhr, and W. Meier, Exp. Fluids **54**, 1532 (2013).
3. Edgewave GmbH, "HD Series Product Datasheet," http://www.edge-wave.de/web/downloads/datenblatter/ (2013).
4. M. N. Slipchenko, J. D. Miller, S. Roy, J. R. Gord, S. A. Danczyk, and T. R. Meyer, Opt. Lett. **37**, 1346 (2012).
5. N. Jiang, M. C. Webster, and W. R. Lempert, Appl. Opt. **48**, B23 (2009).
6. F. Fuest, M. J. Papageorge, W. R. Lempert, and J. A. Sutton, Opt. Lett. **37**, 3231 (2012).
7. J. D. Miller, M. Slipchenko, T. R. Meyer, N. Jiang, W. R. Lempert, and J. R. Gord, Opt. Lett. **34**, 1309 (2009).
8. K. Gabet, R. A. Patton, N. Jiang, W. R. Lempert, and J. A. Sutton, Appl. Phys. B **106**, 569 (2012).
9. J. D. Miller, J. B. Michael, M. N. Slipchenko, S. Roy, T. R. Meyer, and J. R. Gord, Appl. Phys. B **113**, 93 (2013).
10. M. J. Papageorge, T. A. McManus, F. Fuest, and J. A. Sutton, "Recent advances in high-speed planar Rayleigh scattering in turbulent jets and flames: increased record lengths, acquisition rates, and image quality," Appl. Phys. B (to be published).
11. N. Jiang, M. Webster, W. R. Lempert, J. D. Miller, T. R. Meyer, C. B. Ivey, and P. M. Danehy, Appl. Opt. **50**, A20 (2011).
12. M. Slipchenko, J. Miller, S. Roy, J. Gord, and T. Meyer, Opt. Express **21**, 681 (2013).
13. J. M. Grace, P. E. Nebolsine, C. L. Goldley, G. Chahal, J. Norby, and J. M. Heritier, Opt. Eng. **37**, 2205 (1998).
14. C. F. Kaminski, J. Hult, and M. Alden, Appl. Phys. B **68**, 757 (1999).
15. P. P. Wu and R. B. Miles, Opt. Lett. **25**, 1639 (2000).
16. B. Thurow, N. Jiang, M. Samimy, and W. Lempert, Appl. Opt. **43**, 5064 (2004).
17. R. Schefer and P. Goix, Combust. Flame **112**, 559 (1998).
18. L. Muñiz and M. Mungal, Combust. Flame **126**, 1402 (2001).
19. C. Brackmann, J. Nygren, X. Bai, Z. Li, H. Bladh, B. Axelsson, I. Denbratt, L. Koopmans, P.-E. Bengtsson, and M. Aldén, Spectrochim. Acta A **59**, 3347 (2003).
20. N. R. Panchapakesan and J. L. Lumley, J. Fluid Mech. **246**, 225 (1993).
21. T. C. Lieuwen and V. Yang, eds., *Combustion Instabilities in Gas Turbine Engines: Operational Experience, Fundamental Mechanisms, and Modeling* (American Institute of Aeronautics and Astronautics, 2005).